Journal of Power Sources 195 (2010) 6719–6731

Contents lists available at ScienceDirect

Journal of Power Sources

journal homepage: www.elsevier.com/locate/jpowsour

Transient and steady-state analysis of catalyst poisoning and mixed potential formation in direct methanol fuel cells

Dietmar Gerteisen*

Fraunhofer Institute for Solar Energy Systems, Heidenhofstrasse 2, 79110 Freiburg, Germany

ARTICLE INFO

Article history:
Received 6 November 2009
Received in revised form 31 March 2010
Accepted 5 April 2010
Available online 13 April 2010

Keywords:
Fuel cell
DMFC
Crossover
Mixed potential
Overshoot behavior

ABSTRACT

The present dynamic model is developed to investigate the coupled reaction mechanisms in a DMFC and therein associated voltage losses in the catalyst layers. The model describes a complete five-layer membrane electrode assembly (MEA), with gas diffusion layers, catalyst layers and membrane. The analysis of the performance losses are mainly focused on the electrochemical processes. The model accounts for the crossover of both, methanol from anode to cathode and oxygen from cathode to anode. The reactant crossover results in parasitic internal currents that are finally responsible for high overpotentials in both electrodes, so-called mixed potentials. A simplified and general reaction mechanism for the methanol oxidation reaction (MOR) was selected, that accounts for the coverage of active sites by intermediate species occurring during the MOR. The simulation of the anode potential relaxation after current interruption shows an undershoot behavior like it was measured in the experiment [1]. The model gives an explanation of this phenomenon by the transients of reactant crossover in combination with the change of CO and OH coverages on Pt and Ru, respectively.

1. Introduction

Direct methanol fuel cells (DMFCs) have important advantages to hydrogen fuel cells such as the higher energy content of liquid methanol, the simple storage and the simple refilling. Hence, DMFCs are promising candidates for portable power applications. However there are several serious technical problems to overcome for such cells to be competitive in the market. The thermodynamic reversible cell potential for the overall cell reaction of a DMFC is 1.21 V at 298 K [2]. However, the open circuit voltage (OCV) is typically only in the range of 600–750 mV [3–6], depending on the operating conditions, membrane type, catalyst and catalyst loading. The question arises "why"? It is assumed that the relatively high concentration of methanol (compared with gaseous reactants such as oxygen and hydrogen) and the high permeability of the polymer electrolyte membrane combine the possibility of a high flux of methanol to the cathode where it can react with oxygen in an electrochemical reaction. One following consequence is that the electrode on the cathode is always under load even if no external current is drawn from the cell. Thus, the cathode potential is suppressed by the activation overpotential due to the internal parasitic current, quite obvious at OCV. This phenomenon of a deteriorated electrode potential caused by fuel crossover from the anode to the cathode side where methanol is oxidizing on the platinum catalyst is called mixed potential [7–10,6,3]. Further drawbacks of methanol crossover are the waste of fuel and the poisoning of cathodic electrocatalyst. The methanol oxidation reaction has been subject of a large number of studies in recent years [11–14]. The problem of methanol crossover can hardly be solved as long as perfluorosulfonic acid membranes such as Nafion® are used as separator between anode and cathode compartment. The fact that hydration of protons is required for a proper ionic conductivity and that water is needed for the methanol oxidation to CO_2, necessitates that water has always to be present in the anode compartment. Water and methanol are interchangeable in the hydration and osmotic process because the free energy of association with protons is approximately the same for both solvents. This in turn leads to high methanol flux through the membrane causing mixed potential on the cathode side.

To avoid the oxidation of methanol on the cathode several methods have been explored. Possibilities are the development of a novel membrane that prevents or at least reduces the permeation of methanol through the membrane [15,16] or the use of methanol vapor instead of a liquid methanol solution to reduce the amount of dissolved methanol in water at the electrode/membrane interface [17] and therefore the diffusive flux of methanol to the cathode. Another approach to overcome the decrease in cathode performance by methanol crossover is to use a methanol tolerant oxygen reduction electrocatalyst, i.e. an oxygen reduction reaction (ORR) selective catalyst [10,18–20,8]. High methanol tol-

* Corresponding author. Tel.: +49 761 4588 5205; fax: +49 761 4588 9000.
E-mail address: dietmar.gerteisen@ise.fraunhofer.de.

0378-7753/$ – see front matter © 2010 Elsevier B.V. All rights reserved.
doi:10.1016/j.jpowsour.2010.04.004

erance is reported in the literature for non-noble metal catalysts based on chalcogenides and macrocycles of transition metals or platinum-based binary alloyed catalysts [19]. Investigations of the electrocatalytic activity of such catalysts using rotating disc electrode (RDE) measurements in acidic media show cathode potentials up to 1 V [20,19]. In using such catalysts in a fuel cell, an apparent higher OCV should be measured. Nevertheless, the OCV of technical electrodes with methanol tolerant cathode catalysts in DMFCs does not show such high values. Thus, either the anode potential of the methanol oxidation reaction (MOR) is far above the theoretical value of approx. 20 mV versus normal hydrogen electrode [2], or a so far not completely understood coupling between the cathode and anode causes this low OCV despite of a methanol tolerant catalyst. By means of a reference electrode configuration in the test cell, presented by Gerteisen [1], the loss mechanism of a methanol tolerant ruthenium-based catalyst modified with selenium ($RuSe_x$) was investigated using current interrupt measurements (CI). In several publications an overshoot of the cell voltage is measured if there is a sudden load step from a high current to a low current. In most cases the phenomenon is discussed as an interaction between the relaxation of the ORR potential and the methanol crossover building a mixed potential on the cathode side [21,22,9]. In the experiments described in [1], the current interrupt technique was used to prove the methanol tolerance of the $RuSe_x$ catalyst with the reference electrode configuration. The cathode potential relaxation of a CCM prepared with Pt/C as cathode catalyst was compared with a CCM prepared with $RuSe_x$/C (details in [1]). A current density of 0.1 A cm^{-2} was applied before a fast circuit breaker unload the cell. The curve with the Pt catalyst shows an overshoot behavior of the cathode potential, while the $RuSe_x$-based CCM does not show such a behavior. This result indicates a high methanol tolerance of the $RuSe_x$/C catalyst. However, both CCMs show an undershoot behavior of the anode potential.

Presently there are no scientific publications known, which report on monitoring of an anode undershoot relaxation. From the measurements it can be concluded that on the anode side at least two processes with different time constants are taking place and competing with one another. The faster process is responsible for the anode potential decrease to low potentials (favorable for fuel cell application), the second process dominates after some seconds (approx. 6 s) and forces the anode potential to an adverse high potential, at least 100 mV higher as expected from theory.

In the literature, different DMFC models highlighting various physical and electrochemical aspects are published. Shivhare et al. [23] developed a simplified steady-state anode model. The model is focused on the anode kinetics and therefore accounts for the *CO* catalyst poisoning as well as for the water activation by the bi-functional mechanism. The simulation results show that *CO* coverage does not play an important role in the loss mechanism of the anode. Ge and Liu [24] developed a 3D model subjected to mass transport processes in the channel, GDL and CL. The reaction kinetics is modeled as a lumped Tafel approach without considering multi-steps reaction and the influence of residues. A cathodic mixed potential is calculated by the assumption of a leak current due to methanol crossover, implemented in the Tafel equation by adding to the external load current. A similar model in 2D is presented by Yang et al. [25]. The steady-state model from Liu and Wang [26] focused on mixed potential and the influence of surface coverages of *CO* and *OH* only for the cathode. Mass transport limitations are considered in the two-phase formulation. The anode side is not regarded. The effect of pulsed-current load of a DMFC on the performance is investigated by Vilar et al. [27]. Their dynamic model is reduced to the anode side, subjected to a detailed bi-functional methanol oxidation kinetics. The model predicts an undershoot relaxation that is attributed to a small electrical short-circuit though the membrane. For simplification, the electrodes are not spatially resolved.

Regarding the explanations of the cell-voltage overshoot phenomenon given in the literature, they are mostly attributed to mixed potential on the cathode side. Therefore, the main research activities are focused on preventing methanol crossover and parasitic MOR on the cathode. Less concentration is given on the dynamics of the anode kinetics. It is believed that the bi-functional mechanism of a Pt–Ru alloy catalyst is sufficient for the oxidation of methanol to *CO* and further to CO_2 by a hydroxyl ion *OH* but the influence of oxygen crossover to an anode mixed potential has not been investigated so far. In spite of a much lower oxygen flux through the membrane compared to the methanol flux, the resulting parasitic ORR at the anode side can have a strong impact due to the slow anode kinetics, intensified by partially blocked Pt-sites by *CO*.

In the following this phenomena is investigated by a new developed DMFC model that accounts for the crossover of both, methanol from anode to cathode and oxygen from cathode to anode. The bi-functional mechanism is implemented in the anode kinetics. Thus, a fully coupled time-dependent model is realized, predicting mixed potential formation and *CO* poisoning. Qualitative investigations of the anodic potential relaxation are made by numerical modeling that gives an explanation for the anode undershoot behavior. To quantify the anode overpotential further fundamental electrochemical investigations and analysis techniques such as, e.g. gas chromatography and X-ray adsorption spectroscopy have to be conducted, which was not scope of this work.

2. Modeling

The present model is developed to investigate the coupled reaction mechanism of a DMFC and therein associated voltage losses in the catalyst layers. The model accounts for the crossover of (i) methanol from anode to cathode and (ii) oxygen from cathode to anode. The reactant crossover results in parasitic internal currents which finally are responsible for high overpotentials in both electrodes, so-called mixed potentials. A simplified and general reaction mechanism for the MOR derived from a more complex mechanism was selected [28,29], that accounts for the coverage of active sites by intermediate species occurring during the MOR. Additionally, the effect of oxygen crossover to the anode side is implemented, which is a novel approach in DMFC modeling and not yet reported in the appropriate literature.

The model describes a complete five-layer membrane electrode assembly (MEA), with cathode gas diffusion layer (CGDL), cathode catalyst layer (CCL), membrane, anode catalyst layer (ACL) and anode gas diffusion layer (AGDL), as depicted in Fig. 1.

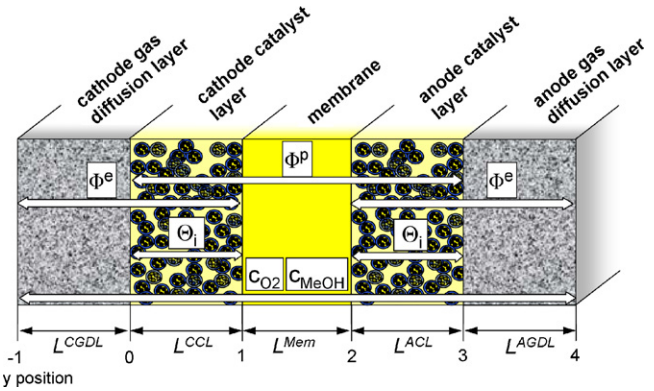

Fig. 1. Schematic of a five-layer membrane electrode assembly. The solving variables are denoted and their computational domains are marked by white arrows.

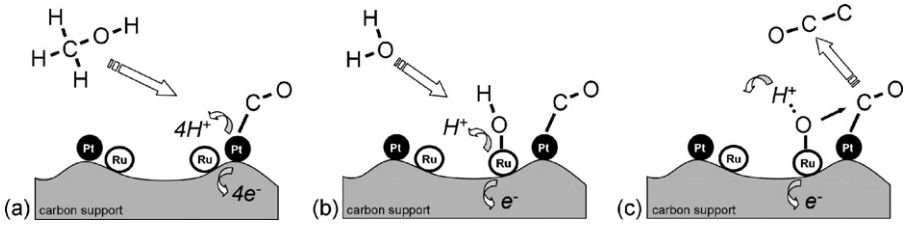

Fig. 2. Bi-functional mechanism of the methanol oxidation reaction on PtRu catalyst: (a) electro-oxidation of methanol to carbon monoxide, (b) water activation forming hydroxyl (*OH*) radicals, (c) electro-oxidation of *CO* by an *OH*-radical.

In this model performance losses are mainly addressed to electrochemical processes. For simplification, the gas diffusion electrode is modeled as a homogeneous catalyst layer, where details on the electrode morphology, i.e. agglomerate approach [30–33], are neglected. Although under these assumptions mass transport losses are not correctly represented, the model does not loose its significance because the electrochemical phenomena such as mixed potential and catalyst poisoning are the determining loss mechanism in DMFCs [34].

Since the limiting current density of DMFCs is significantly lower compared to H_2-PEFCs on a two-phase flow description concerning liquid water in the cathodic porous media and on CO_2-bubble formation on the anode were passed.

2.1. Reaction mechanism

The model description starts with the assumptions of the basic reaction processes occurring in the electrodes.

2.1.1. Oxygen reduction reaction

The desired reaction in the CCL is the oxygen reduction reaction. The simplest description for its kinetics in acidic environment is a four-electron step mechanism after adsorption on an active site

$$O_2 + (\mathrm{Pt}) \underset{k_{O_2,des}}{\overset{k_{O_2,ads}}{\rightleftharpoons}} (\mathrm{Pt} - O_2), \tag{1}$$

$$(\mathrm{Pt} - O_2) + 4H^+ + 4e^- \overset{k_{ORR}}{\rightleftharpoons} 2H_2O + (\mathrm{Pt}), \tag{2}$$

where the reaction is catalyzed by platinum catalyst.

It is assumed that the ORR is not restricted to the CCL. A Nafion®-based membrane shows a low but not negligible gas permeability. This leads to the situation that a small amount of dissolved oxygen diffuses through the membrane to the anode side, where it also can be reduced on free Pt-sites following reactions (1) and (2).

2.1.2. Methanol oxidation reaction

It is widely accepted that during methanol oxidation reaction, first methanol adsorbs on a Pt catalyst site and then oxidizes. Unfortunately, methanol does not oxidize to CO_2 in a single step. One intermediate of the reaction is carbon monoxide *CO* that remains as residue on the catalyst site. The latter is inactive for further reactions as long as the *CO*-adsorbate blocks the catalyst. This phenomenon is called *CO*-poisoning. An appreciable blocking by other intermediates such as CH_2OH, $CHOH$, CHO, acting as catalyst poison, is not reported in the literature. Thus, the reaction of methanol to *CO* is assumed as rate-determining step

$$CH_3OH + (\mathrm{Pt}) \underset{k_{M,des}}{\overset{k_{M,ads}}{\rightleftharpoons}} (Pt - CH_3OH), \tag{3}$$

$$(Pt - CH_3OH) \underset{k'_{MOR}}{\overset{k_{MOR}}{\rightleftharpoons}} (Pt - CO) + 4H^+ + 4e^-. \tag{4}$$

Ruthenium is mostly added to Pt as co-catalyst on the anode side to promote the bi-functional mechanism, proposed by Watanabe and Motoo [35]. Fig. 2 gives an illustration of the bi-functional MOR mechanism, described in subsection 1. It is assumed that the catalytic activity of Pt for the MOR is at least two orders of magnitude higher then Ru. Therefore, the electro-oxidation of methanol on Ru is neglected. A bi-functional catalyst, like Pt–Ru alloy catalyst, enhance the *CO* oxidation reaction (COOR) [35]. The Ru catalyst activates water molecules to hydroxyl radicals (reaction (5)), which react with *CO* adsorbates to carbon dioxide CO_2 (reaction (6)). Here, it is assumed that water preferentially adsorbs onto Ru-sites

$$H_2O + (\mathrm{Ru}) \underset{k_{OH,red}}{\overset{k_{H_2O,ox}}{\rightleftharpoons}} (Ru - OH) + H^+ + e^-, \tag{5}$$

and that the adsorbed *OH* species are mobile enough to reach the Pt-sites where *CO* become oxidized

$$(Pt - CO) + (Ru - OH) \overset{k_{CO,ox}}{\longrightarrow} CO_2 + H^+ + e^- + (\mathrm{Pt}) + (\mathrm{Ru}). \tag{6}$$

Due to the missing Ru catalyst in the cathode CL, reaction (5) is not present on the cathode side.

A second possible reaction pathway is the heterogeneous oxidation of *CO* to CO_2 in case of accessible oxygen. This reaction pathway is often utilized in hydrogen PEFC fed with reformat gas, where *CO* is present in the range of several *ppm*. In giving a small amount of oxygen into the hydrogen reformat feed stream, the *CO*-poisoning of the anode catalyst gets significantly reduced (known as oxygen bleeding) by a heterogeneous oxidation reaction [36]. This reaction is also addressed in the model for the *CO* adsorbate at the Pt-sites

$$2(Pt - CO) + O_2 \overset{k_{bleed}}{\longrightarrow} 2CO_2 + (2\mathrm{Pt}). \tag{7}$$

Without assuming this heterogeneous reaction, there is no possibility to clean the Pt catalyst from *CO* on the cathode side, since no Ru catalyst is available to form *OH*-species for further oxidation. Consequently, the methanol oxidation on the cathode would poison the active sites by-and-by until no current can be drawn from the cell. Obviously this scenario does not occur in real DMFCs, confirming the assumed reaction pathway (7).

2.2. Governing equations

The model based on a system of coupled partial differential equations, whereby continuity equations for eight variables have to be solved. The solving variables are oxygen concentration c_{O_2}, methanol concentration c_M, electronic potential Φ^e, protonic potential Φ^p and surface coverages of oxygen Θ_{O_2}, methanol Θ_M, carbon monoxide Θ_{CO} and hydroxyl ions Θ_{OH}.

The concentrations are defined in all five layers, the electronic potential is defined in the electronic conductive regions (CLs and GDLs), the surface coverages are defined in the CLs and the protonic potential is defined in the layers where ionomer is present, namely the CLs and the membrane (denoted by white arrows in Fig. 1).

2.2.1. Reaction rates

The volumetric reaction rates describe the conversion of the reactants and intermediates dependent on their kinetic parameters, coverages and applied overpotentials.

The oxygen reduction reaction can be described by Butler–Volmer kinetics, where only adsorbed oxygen on the Pt-sites, expressed as Θ_{O_2}, takes part in the reaction

$$q_{ORR} = \gamma_{c,a} k_{ORR}\, e^{(73.2\times10^3/R)((1/353)-(1/T))}\Theta_{O_2} \times \left(e^{(\Phi^e-\Phi^p-\Delta\Phi^0_{ORR})/b^*_{ORR}} - e^{-(\Phi^e-\Phi^p-\Delta\Phi^0_{ORR})/b_{ORR}} \right). \quad (8)$$

The temperature dependent Tafel slope for the ORR is defined as

$$b^*_{ORR} = \frac{(1-\alpha_{ORR})n_{ORR}F}{RT} \quad \text{and} \quad b_{ORR} = \frac{\alpha_{ORR}n_{ORR}F}{RT}, \quad (9)$$

where α_{ORR} is the symmetry factor, n_{ORR} the number of transfered electrons, F the Faraday constant, R the gas constant and T the temperature. Thus the assumed oxygen reduction reaction depends on the reaction constant k_{ORR}, the Tafel slope of the ORR, the reversible potential $\Delta\Phi^0_{ORR}$ of the ORR, the catalyst loading $\gamma_{c,a}$ and the applied overpotential, determined by Φ^e and Φ^p, which are the potentials in the electronic and ionic conductive phase, respectively.

The reaction constant k_{ORR} as well as all following reaction constants k_i are functions of the catalyst type (CT), catalyst support (CS) and the active surface area (A), which in turn depends on the loading and dispersion of the catalyst and the three-phase boundary formation

$$k_i = k_i(\text{CT,CS,A}). \quad (10)$$

Therefore the published values differ strongly, depending on the electrode system and preparation. In this model a simple constant is used merging all mentioned characteristics. A semi-empirical adsorption isotherm, known as Frumkin isotherm, is assumed for the description of the oxygen adsorption process in the catalyst layer. The Frumkin isotherm takes the interaction between the adsorbed species into account

$$q_{O_2,ads} = \gamma_{c,a} k_{O_2,ads}(1-\Theta_{O_2}-\Theta_{CO}-\Theta_M)c_{O_2}\, e^{-g_1\Theta_{O_2}}, \quad (11)$$

where the dimensionless constant g_1 is a measure of the mean interaction energy (attraction constant). Adsorption only takes place at free catalyst sites, expressed as $\left(1-\sum_i \Theta_i\right)$.

It is assumed that methanol oxidizes in a four-electron step mechanism to *CO*, preferentially on Pt-sites. This leads to a Butler–Volmer expression

$$q_{MOR} = \gamma_{c,a} k^*_{MOR}\Theta_M\, e^{(\Phi^e-\Phi^p-\Delta\Phi^0_{MOR})/b^*_{MOR}} - \gamma_{c,a} k'_{MOR}\Theta_{CO}\, e^{-(\Phi^e-\Phi^p-\Delta\Phi^0_{MOR})/b_{MOR}}, \quad (12)$$

where

$$k^*_{MOR} = k_{MOR}\, e^{-((98.3\times10^3)/RT)}, \quad (13)$$

where Θ_M and Θ_{CO} are the methanol and carbon monoxide surface coverage, respectively, $b^*_{MOR} = ((1-\alpha_{MOR})n_{MOR}F)/RT$ and $b_{MOR} = (\alpha_{MOR}n_{MOR}F)/RT$ are the Tafel slopes of the MOR. The values of the reversible potential of the MOR $\Delta\Phi^0_{MOR}$, the symmetry factor α_{MOR} and the reaction rates (k_{MOR}, k'_{MOR}) are listed in Table 1.

Again, the methanol adsorption is expressed as Frumkin isotherm

$$q_{M,ads} = \gamma_{c,a} k_{M,ads}(1-\Theta_{O_2}-\Theta_{CO}-\Theta_M)c_M\, e^{-g_2\Theta_M} - \gamma_{c,a} k_{M,des}\Theta_M\, e^{g_2\Theta_M}, \quad (14)$$

where $k_{M,ads}$ and $k_{M,des}$ are the rate constants for the adsorption and desorption process.

The hydroxyl ion formation onto Ru catalysts, also called water activation, is coupled with an electron transfer, which can also be expressed by the Butler–Volmer expression

$$q_{act} = k^*_{H_2O,ox}(1-\Theta_{OH})\, e^{(\Phi^e-\Phi^p-\Delta\Phi^0_{OH})/b^*_{act}} - k^*_{OH,red}\Theta_{OH}\, e^{-(\Phi^e-\Phi^p-\Delta\Phi^0_{OH})/b_{act}}, \quad (15)$$

where

$$k^*_{H_2O,ox} = k_{H_2O,ox}\, e^{(73.6\times10^3)/RT} \quad (16)$$

$$k^*_{OH,red} = k_{OH,red}\, e^{-(25.4\times10^3)/RT} \quad (17)$$

are the temperature dependent rate constants for the forward and reverse reaction, respectively, $\Delta\Phi^0_{OH}$ is the equilibrium potential, $b^*_{act} = ((1-\alpha_{act})n_{act}F)/RT$ and $b_{act} = (\alpha_{act}n_{act}F)/RT$ are the Tafel slopes of the water activation reaction. The adsorption process of water prior to the activation is not explicitly modeled, valid for fast adsorption rates.

A Langmuir-Hinshelwood mechanism is assumed for the *CO* oxidation by hydroxyl ions, which strongly depends on the potential modeled with a simple Tafel expression

$$q_{COOR} = k^*_{CO,ox}\Theta_{CO}\Theta_{OH}\, e^{(\Delta\Phi^0_{COOR}-(\Phi^e-\Phi^p))/b_{COOR}}, \quad (18)$$

where

$$k^*_{CO,ox} = k_{CO,ox}\, e^{-(12.6\times10^3)/RT} \quad (19)$$

is the reaction rate constant, $b_{COOR} = ((1-\alpha_{COOR})n_{COOR}F)/RT$ the corresponding Tafel slope and $\Delta\Phi^0_{COOR}$ the equilibrium potential.

The heterogeneous oxidation of *CO* with O_2 is modeled according to a Langmuir-Hinshelwood mechanism

$$q_{bleed} = k_{bleed}\Theta_{O_2}(\Theta_{CO})^2\, e^{-(90\times10^3)/RT}, \quad (20)$$

where an Arrhenius expression with a reaction rate constant k_{bleed} is chosen to count for the temperature dependance.

2.2.2. Oxygen concentration

Oxygen enters the five-layer MEA at the cathode GDL, diffuses to the cathode catalyst layer, where it dissolves into the ionomer to reach the active sites for the ORR. If not all oxygen is consumed in the cathode CL, that means there is an oxygen concentration unequal to zero at the interface CL ↔ membrane, the dissolved oxygen can diffuse through the membrane forced by a concentration gradient between cathode and anode CL.

The oxygen flux in gaseous $j^g_{O_2}$ and dissolved phase $j^d_{O_2}$ is modeled by simple Fick's diffusion

$$j^{g,d}_{O_2} = -\frac{D^{eff,\Omega}_{O_2}}{L^\Omega}\frac{\partial c^{g,d}_{O_2}}{\partial y}, \quad (21)$$

where $D^{eff,\Omega}_{O_2}$ is the effective diffusion coefficient in domain Ω

$$D^{eff,\Omega}_{O_2} = \begin{cases} D^g_{O_2}((1-s)\epsilon^\Omega_{O_2})^{1.5}\left(\frac{T}{353}\right)^{1.5} & \text{if} \quad \Omega = \text{CGDL} \wedge \text{CGL}, \\ D^d_{O_2} & \text{if} \quad \Omega = \text{Mem} \wedge \text{ACL}, \end{cases} \quad (22)$$

where L^Ω denotes the thickness of the layer Ω since the model domains are normalized to one. In the porous media a Bruggeman expression accounts for the reduced diffusion pathway by the solid matrix and water saturation. Since the diffusion process of dissolved oxygen in the ionomer is of several magnitudes slower than for gaseous oxygen in the open gas pores, the oxygen diffusion in the CL is modeled only in gaseous phase. The local distributed gaseous oxygen $c^g_{O_2}$ in the CL is converted to the dissolved oxygen concentration $c^d_{O_2}$ by Henry's law

$$c^d_{O_2} = Hc^g_{O_2}, \quad (23)$$

where H is the Henry constant.

Taking the oxygen adsorption process and the heterogeneous *CO*-oxidation into account, mass balance equation yields

$$\frac{\partial j^{g,d}_{O_2}}{\partial y} = L^{\Omega}\left(q^{\Omega}_{O_2} - \epsilon^{\Omega}_{O_2}\frac{\partial c^{g,d}_{O_2}}{\partial t}\right) \tag{24}$$

whereas the sink terms are defined only in the catalyst layers

$$q^{\Omega}_{O_2} = \begin{cases} -q_{O_2,ads} - q_{bleed} & \text{if} \quad \Omega = CCL \wedge ACL, \\ 0 & \text{if} \quad \text{else}, \end{cases} \tag{25}$$

and $\epsilon^{\Omega}_{O_2}$ is the fraction of space accessible for the oxygen in layer Ω. The accumulation term in the CCL accounts only for the gaseous oxygen concentration, i.e. $\epsilon^{\Omega}_{O_2} = \epsilon^{\Omega}_{p}$. In the membrane and ACL $\epsilon^{\Omega}_{O_2}$ is the ionomer fraction and pore space, since oxygen is dissolved in the water and ionomer in these domains.

2.2.3. Methanol concentration

The anode is fed with methanol via the anode GDL, from where methanol has to diffuse towards the anode catalyst layer, reaching active sites. Due to the use of an aqueous methanol solution, a concentration discontinuity between methanol in the secondary pores and in the primary pores is neglected. Methanol crossover is assumed in the case of a finite methanol concentration at the interface ACL ↔ membrane. The methanol flux j_M is modeled by Fick's diffusion and forced by the electro-osmotic drag

$$j_M = -\frac{D^{eff,\Omega}_M}{L^{\Omega}}\frac{\partial c_M}{\partial y} - \frac{j_p \alpha_{drag}}{F}, \tag{26}$$

with the electro-osmotic drag coefficient

$$\alpha_{drag} = \frac{2.5\lambda}{22}\zeta, \tag{27}$$

where

$$\zeta = \frac{c_M}{(((1-c_M)\nu_M)/\nu_{H_2O}) + c_M} \tag{28}$$

accounts for the fraction of methanol in the aqueous solution dragged by the protons instead of water molecules. In the transport equation, $D^{eff,\Omega}_M$ is the effective diffusion coefficient of methanol, j_p the local current density, α_{drag} the electro-osmotic drag coefficient, $\lambda = 22$ the water content (water molecules per sulphonic acid sites) of a fully hydrated ionomer and ν_i the molar volume of species *i*. Again a Bruggeman correction term is used for the effective diffusion coefficient

$$D^{eff,\Omega}_M = \begin{cases} \epsilon_i^{1.5} D_M & \text{if} \quad \Omega = \text{CCL} \wedge \text{Mem}, \\ (\epsilon_i + \epsilon_p)^{1.5} D_M & \text{if} \quad \Omega = \text{ACL}, \\ \epsilon_p^{1.5} D_M & \text{if} \quad \Omega = \text{AGDL}. \end{cases} \tag{29}$$

Methanol mass conservation equation can be expressed by

$$\frac{\partial j_M}{\partial y} = L^{\Omega}\left(q^{\Omega}_M - \epsilon^{\Omega}_M \frac{\partial c_M}{\partial t}\right), \tag{30}$$

where the sink terms are only defined in the catalyst layers

$$q^{\Omega}_M = \begin{cases} q_{M,ads} & \text{if} \quad \Omega = \text{CCL} \wedge \text{ACL}, \\ 0 & \text{if} \quad \text{else}, \end{cases} \tag{31}$$

and ϵ^{Ω}_M is the volume fraction in layer Ω where methanol is present.

2.2.4. Surface coverage

The transient surface coverage of O_2, *MeOH*, *CO* onto Pt and *OH* onto Ru are described by ordinary differential Eqs. (32)–(35):

$$\Gamma_{Pt}\frac{\partial \Theta_{O_2}}{\partial t} = +q_{O_2,ads} - q_{ORR}, \tag{32}$$

$$\Gamma_{Pt}\frac{\partial \Theta_{MeOH}}{\partial t} = +q_{M,ads} + q_{MOR}, \tag{33}$$

$$\Gamma_{Pt}\frac{\partial \Theta_{CO}}{\partial t} = -q_{COOR} - 2q_{bleed} - q_{MOR}, \tag{34}$$

$$\Gamma_{Ru}\frac{\partial \Theta_{OH}}{\partial t} = +q_{act} - q_{COOR}, \tag{35}$$

where Γ_i is the active site density of catalyst *i*.

2.2.5. Electronic and protonic potential

Ohm's law is used for the description of the charge flux

$$j_{p/e} = \mp\frac{\sigma^{eff,\Omega}_{p/e}}{L^{\Omega}}\frac{\partial \Phi^{p/e}}{\partial y}, \tag{36}$$

where the subscript p/e stands for protons and electrons. The ionic conductivity of the ionomer σ_p is a strong function of the water content for which Springer et al. [37] has found an analytical expression (Eq. (37)). Since the water content is not calculated in the model a constant value of 22 is assumed, that corresponds to an equilibrium value of a saturated membrane in liquid environment which is fulfilled in the anode compartment fed with aqueous methanol solution

$$\sigma^{eff,\Omega}_p = (\epsilon^{\Omega}_i)^{1.5}(0.514\lambda - 0.326)\, e^{1268((1/303)-(1/T))} \quad \text{with} \quad \lambda = 22. \tag{37}$$

A Bruggeman correction accounts for the ionomer fraction ϵ^{Ω}_i in layer Ω.

The charge balance equation reads

$$\frac{\partial j_{p/e}}{\partial y} = L^{\Omega}\left(q^{\Omega}_{p/e} + C_{DL}\frac{\partial(\Phi^e - \Phi^p)}{\partial t}\right), \tag{38}$$

where $q^{\Omega}_{p/e}$ are the volumetric charge transfer rates defined as

$$q^{\Omega}_{p/e} = \begin{cases} F(4q_{ORR} + 4q_{MOR} + q_{COOR} + q_{act}) & \text{if} \quad \Omega = \text{CCL} \wedge \text{ACL} \\ 0 & \text{if} \quad \text{else}, \end{cases} \tag{39}$$

and C_{DL} is the double layer capacity that accounts for dis-/charge current when the Galvani potential changed.

2.3. Boundary conditions

The following boundary conditions are chosen for the boundary value problem.

2.3.1. Oxygen concentration $c^{g}_{O_2}$

A fix oxygen concentration at the outer surface of the cathode GDL is assumed, calculated by the ideal gas law at atmospheric pressure ($p = 1.01325 \times 10^5$ Pa)

$$c^{g}_{O_2}[-1] = \frac{p}{RT}. \tag{40}$$

Oxygen dissolves into the hydrated ionomer within the cathode CL, described by Henry's law, where it can react on active sites or diffuse towards the anode. If not all oxygen is reduced at the cathode and anode CL, respectively, a Cauchy-type boundary condition is chosen for the outflow

$$j^{d}_{O_2}[3] = \Omega_{O_2} c^{d}_{O_2}[3]. \tag{41}$$

2.3.2. Methanol concentration c_M

Similar boundary conditions are chosen for the methanol concentration as for the oxygen concentration. Depending on the

molarity of aqueous methanol solution, a defined concentration is assumed at the anode inlet

$$c_M[4] = c_M^{molarity}. \quad (42)$$

Not oxidized methanol can leave the cathode CL

$$j_M[0] = \Omega_M c_M[0]. \quad (43)$$

2.3.3. Electronic potential Φ^e

Like in the experiments the simulated DMFC is operated in potentiostatic mode. Thus, the cathode potential is set to the cell voltage U_{cell} on the outer surface of the CGDL

$$\Phi^e[-1] = U_{cell}, \quad (44)$$

and the anode potential is set to zero

$$\Phi^e[4] = 0. \quad (45)$$

2.3.4. Protonic potential Φ^p

Since the protons are not allowed to penetrate into the GDLs on the cathode and anode side, their fluxes are taken to zero at the interfaces CL ↔ GDL

$$\frac{\partial \Phi^p[0]}{\partial y} = \frac{\partial \Phi^p[3]}{\partial y} = 0. \quad (46)$$

2.4. Numerical details

The governing equations are solved using COMSOL Multiphysics™, a commercial software package based on finite element methods. A direct Linear System Solver (UMFPACK) and quadratic Lagrange polynomials as test functions are used. The solver is allowed to take free time steps. The five model domains are discretized with non-uniform grid of 611 elements whereas the interface regions between the domains are meshed with smaller elements.

3. Results and discussion

The aim of this model is to give an explanation of the experimental results presented by Gerteisen [1]. The simulation results reproduce qualitatively the effects of mixed potentials which in turn can explain the observed behavior of the dynamic anode potential relaxation at various operating conditions. The model prediction of this dynamic behavior indicates that the impacts of multi-step reactions, bi-functional mechanism and mixed potential formation are essential in DMFC modeling.

3.1. Polarization curves

Before the dynamic simulations with a methanol tolerant $RuSe_x$ catalyst get discussed, a short excursion to steady-state simulations of polarization curves is given, whereby a non-methanol tolerant catalyst such as platinum is assumed as cathode catalyst. This means, that the same activity of the anode and cathode catalyst towards MOR is assumed, likewise for the activity towards the ORR but certainly with a higher value than for the MOR. If nothing else is stated all shown results are simulated at a temperature of 81 °C.

Simulated polarization curves of both electrodes and the cell voltage are plotted in Fig. 3. Even though the theoretical values of 1.23 V and 21 mV are used as equilibrium potential of the ORR and MOR in the model, the voltage-current curve starts with an OCV of about 640 mV, highlighting the drastic influence of mixed potentials. The cell voltage shows an exponential decline in the activation controlled region, that can be completely attributed to the characteristics of the anode overpotential. The anode overpotential shows an offset of 130 mV at no-load condition, which is about 110 mV above the theoretical value, affected by a parasitic ORR due to oxygen crossover. A strong mass transport controlled region is visible at about 0.23 A cm^{-2}.

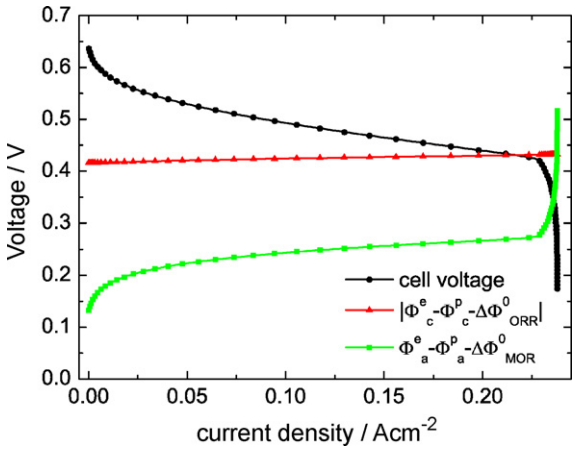

Fig. 3. Simulated polarization curves of the anode and cathode predict mixed potential formation on both electrodes resulting in a low OCV of the voltage–current curve. An exponential increase of the cathode overpotential with current density is not observable.

The cathode overpotential shows a nontypical linear function of current density with a slight slope and an offset of 420 mV at OCV. This result shows that the cathode suffers strongly by a parasitic internal current due to methanol crossover. An explanation for this nontypical cathode behavior can be given by the schematic depicted in Fig. 4(a). The three dashed curves show the typical exponential characteristics of the cathode overpotential with current generation for different fixed parasitic currents. The fact of a parasitic MOR on the cathode needs an ORR to counterbalance the involved charge generation, hence the cathode is under load even no external current is drawn. The largest overpotential is observed for the blue curve due to the high parasitic current. Since the parasitic current is a function of the methanol crossover which decreases with increasing methanol consumption on the anode, the apparent cathode overpotential (red curve) has to be between the blue curve (low current → high fuel crossover) and the black curve (high current → no crossover) depending on the external drawn cell current. Thus the typical exponential shape of the cathode overpotential is lost for such conditions. Measurements published by Eccarius et al. [38] approve such cathode characteristics (Fig. 4(b)).

The reduced OCV and the low performance of the DMFC with the platinum cathode catalyst can be analyzed by the potential and methanol distribution within the fuel cell, plotted in Figs. 5 and 6. It is shown that at open circuit condition the potential difference between the anodic electronic potential Φ^e_a and protonic potential Φ^p is much higher than the theoretical value of 21 mV. Because the electronic potential Φ^e_a is set to zero at the surface of the anode GDL by the boundary condition (like it is done in the experiment by the potentiostat) the protonic potential falls to negative values relative to Φ^e_a. The higher activation losses can be assigned to the cathode. Due to the high electrical conductivity of the GDL and carbon support in the CL the potential gradient ($\nabla\Phi^e$) across these layers can not be seen in this figure. At the highest current density of 0.2 A cm^{-2} a small ohmic drop is observable across the membrane.

The methanol concentration across the cell as a function of the current density is visualized in Fig. 6(a). It shows that methanol is completely oxidized in the cathode CL. Due to the high mass transport limitation of methanol in the anode GDL the methanol crossover to the cathode side decreases with increasing current density. According to this Fig. 6(b) depicts the decreasing parasitic MOR on the cathode side with increasing load. The plot highlights

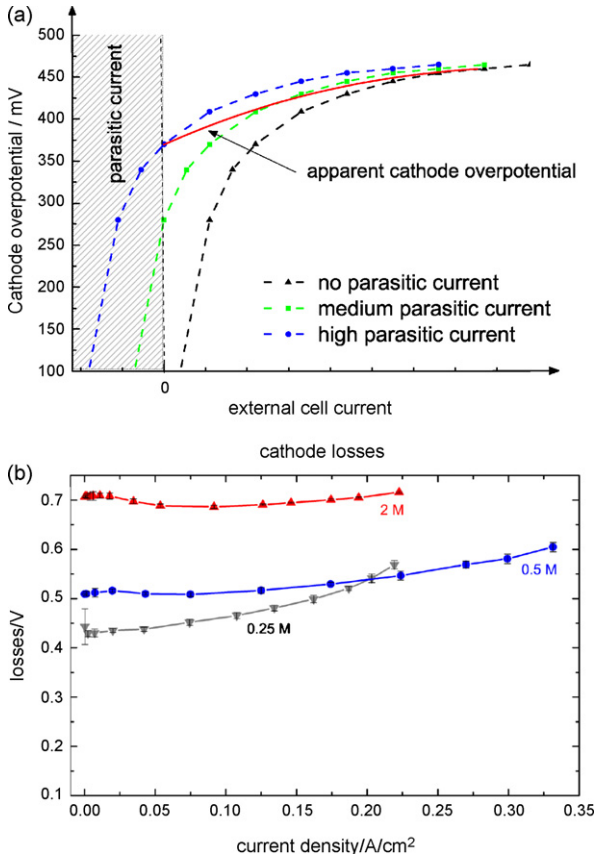

Fig. 4. The cathode overpotential shows a nontypical linear function of current density due to high parasitic MOR on the cathode depending on the load conditions. (a) Schematic of the cathode overpotential under load for different constant parasitic currents. The apparent cathode overpotential accounts for the change off parasitic currents under different load conditions. (b) Measured cathode losses for different molarities (2, 0.5, and 0.25 M) published by S. Eccarius (taken from [38]) approve the linear characteristics of the cathode overpotential.

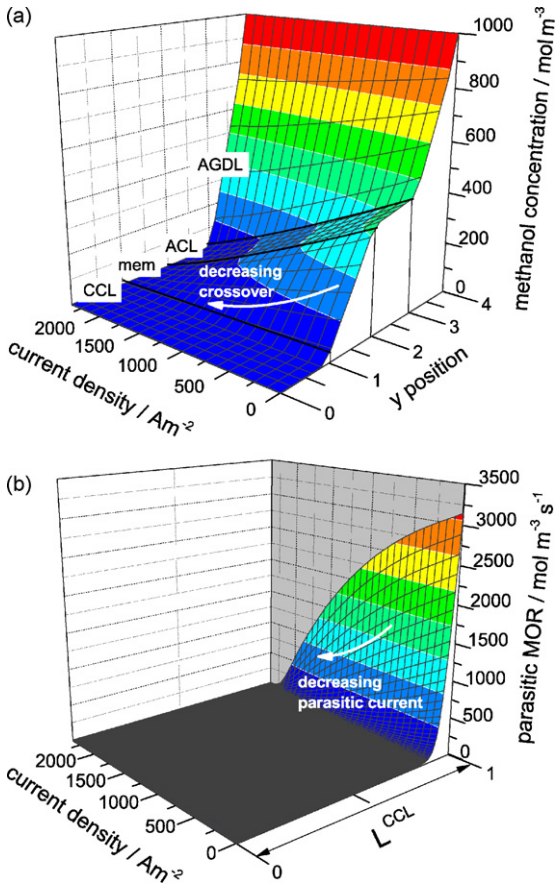

Fig. 6. The methanol crossover and hence the parasitic MOR on the cathode side decreases with increasing current density due to mass transport limitation of methanol in the anode GDL. (a) Methanol concentration profile within the fuel cell as a function of the current density. (b) Methanol completely oxidizes within the first 10% of the CCL due to the extremely high consumption rate at high overpotential.

that the MOR takes place within the first 10% of the CCL at the interface to the membrane due to the high overpotential for the MOR present on the cathode side.

In Fig. 7 the polarization curves of a DMFC based on a high methanol-tolerant cathode catalyst such as $RuSe_x$ are plotted. It is assumed that the activity of the $RuSe_x$ catalyst towards MOR is several magnitudes smaller than the activity of a Pt catalyst ($k_{MOR}^{RuSe} = 10^{-9}\, k_{MOR}^{Pt}$), but unequal to zero. Additionally, it is well known and thus considered in the simulation, that the $RuSe_x$ catalyst shows a relative low activity for the ORR compared to Pt. The model parameter used for the simulations are listed in Table 1.

The exponential shape of the cathode overpotential shows that there is little parasitic MOR at this electrode, contrary to the case with the Pt catalyst (see Fig. 3). Nevertheless, the assumed low activity of the $RuSe_x$ catalyst for the ORR leads to a steep increase in the cathode overpotential when an external cell current is drawn,

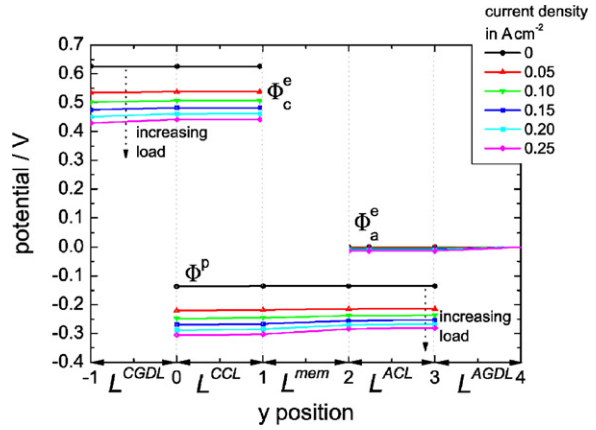

Fig. 5. Simulated potential distribution across the membrane electrode assembly. Both the parasitic methanol oxidation on the cathode and the parasitic oxygen reduction on the anode lead to a reduced cell voltage.

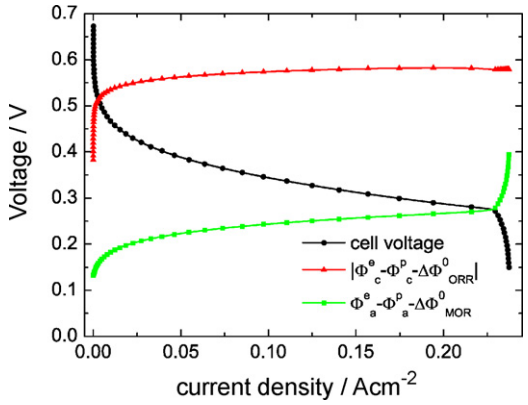

Fig. 7. Simulated polarization curves with $RuSe_x$ as cathode catalyst. Due to the methanol tolerance of $RuSe_x$ the cathode overpotential shows an exponential increase with current, contrary to the overpotential with Pt catalyst shown in Fig. 3.

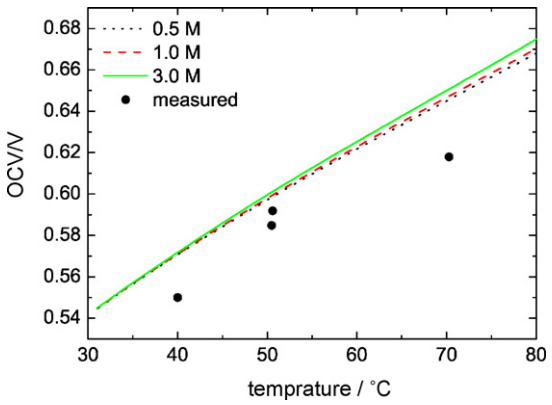

Fig. 8. Comparison of the simulated and measured OCV at different temperatures. The simulation predicts the measured increase of OCV with increasing temperature, but with a small shift 20 mV towards higher voltages.

which in turn leads to comparable performance of a non methanol-tolerant catalyst with high activity for the ORR such as platinum. The assumed small parasitic methanol oxidation on the cathode catalyst together with the fact of a lowered activity towards ORR (compared to Pt) results in a significant cathode mixed potential formation. Both mixed potentials on anode and cathode leads to the low OCV of 620 mV at 60 °C.

Measured OCVs at different temperatures show an increase with temperature, depicted in Fig. 8. The same characteristic is also given by the model. The simulated OCVs predict a slight offset of about 20 mV, towards higher cell voltages compared to the experimental data. Although the kinetic model parameters are not well adjusted (fitted) to experimental data, the temperature dependancy shows a good agreement since the temperature is a sensitive parameter involved in all Arrhenius approaches. The OCV is nearly independent on methanol concentration for the $RuSe_x$ catalyst.

3.2. Dynamic simulations

A further benchmark for the developed model is to reproduce the measured transient response of the anode and cathode potential in a qualitative manner. The overshoot of the cathode potential observed with a Pt-based cathode catalyst should vanish for a methanol-tolerant catalyst like it was measured for $RuSe_x$ [1], whereby the anode undershoot is present for both CCMs. The simulated characteristics of the anode undershoot behavior on switching to no-load should depend on the load current and the inlet methanol concentration like it was measured in the experiment (Fig. 9). In Fig. 10 the simulated relaxation curves of the anode and cathode potential together with the cell voltage is shown for both cathode catalysts, Pt and $RuSe_x$. The anode undershoot is identical for both cases, indicating that the cathode catalyst does not impact the anode side. The cathode overpotential shows a small undershoot in case of Pt catalyst due to methanol crossover which in turn results in parasitic currents. The overpotential with the oxygen-selective $RuSe_x$ catalyst shows a slow transient without an undershoot. Steady-state is not reached with 35 s. The simulated characteristics are in qualitative agreement with the experimental data.

In Fig. 11(a) simulated anode potential relaxation curves for different load currents are shown. In agreement with the measurements the magnitude of the anode undershoot first increases with the load current and finally ends up in an asymptotic behavior for higher currents. The time to reach equilibrium also increases with the load current.

In Fig. 11(b) the anode polarization relaxation after CI at 0.1 A cm^{-2} is shown for different molarities. The anode overpotentials under load vary slightly for different molarities. After CI the undershoot to the lowest anode potential is observed for the highest molarity that ends with the longest relaxation time at the lowest steady-state level. The magnitude of the undershoots are among each other comparable which is not in agreement with the experimental data.

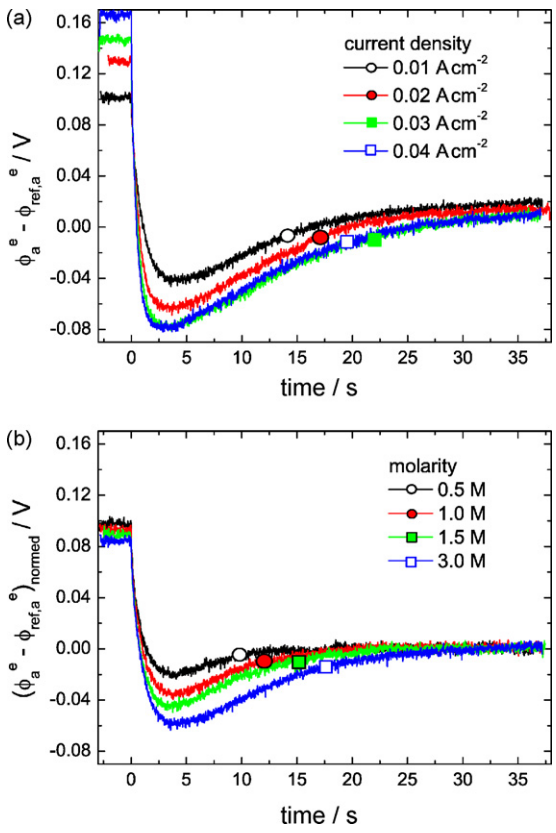

Fig. 9. Measured relaxation curves of the anode polarization for different load current and molarity are shown. Since the change in molarity effects also the reference potential, the steady-state anode potentials are normalized to zero for comparison of their transients. (a) A higher load before current interruption leads to a larger anode potential undershoot, whereby a saturation is reached at 0.04 A cm^{-2}. (b) A higher methanol concentration also leads to an enlarged undershoot behavior with larger relaxation times.

An explanation of the presented anode potential relaxation can be given by mixed potential formation combined with *CO* catalyst poisoning depicted in Fig. 12. Under load the *OH* promotion on the Ru-sites is sufficient for the further oxidation of *CO* to CO_2 because

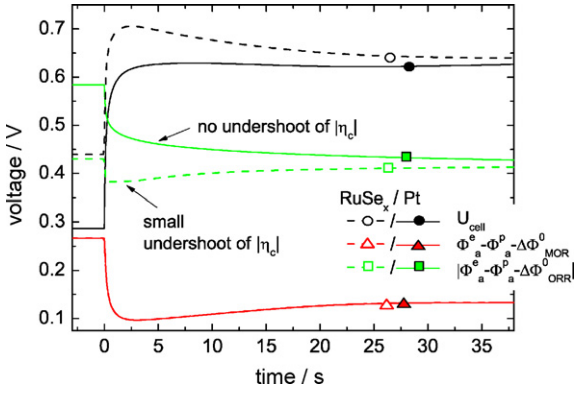

Fig. 10. Potential relaxation curve of the cathode and anode from a load current of 0.2 A cm^{-2}. The cathode overpotential with platinum as cathode catalyst differs significantly from the overpotential with $RuSe_x$ catalyst.

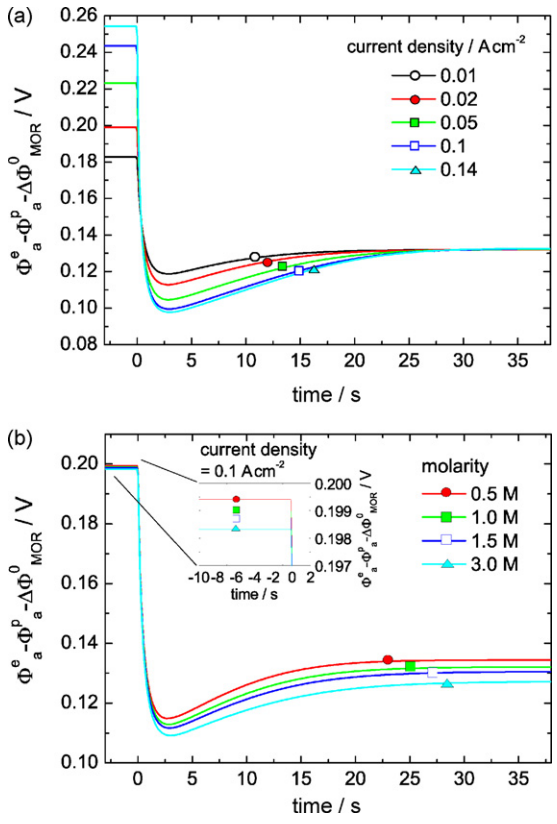

Fig. 11. The impact of the load current and methanol molarities on the transient response after CI is analyzed. (a) The minima of anode relaxation curves for different load currents predict an asymptotic saturation for higher currents. (b) Dependancy of the anode potential relaxation curve on the inlet methanol concentration. The higher molarity improves the steady-state potential.

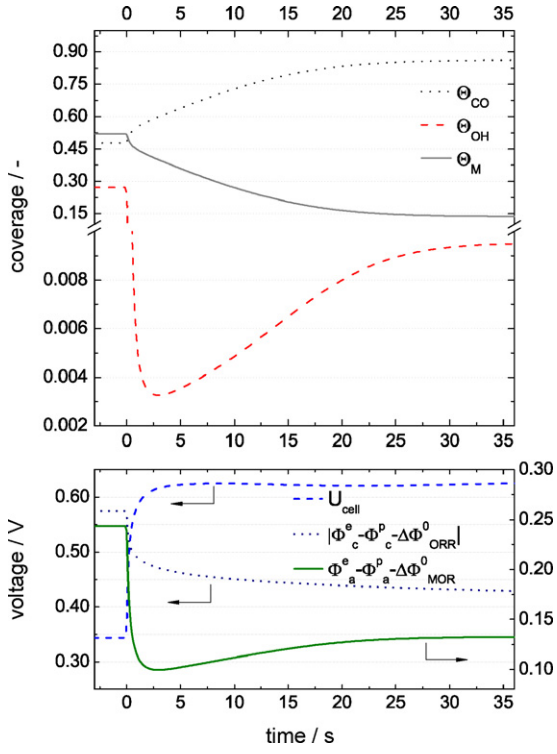

Fig. 12. The anode undershoot behavior is caused by the dynamic change of the *CO* adsorbate in the anode catalyst layer. The high poisoning at no-load condition leads to mixed potential formation due to a low parasitic ORR on the anode side.

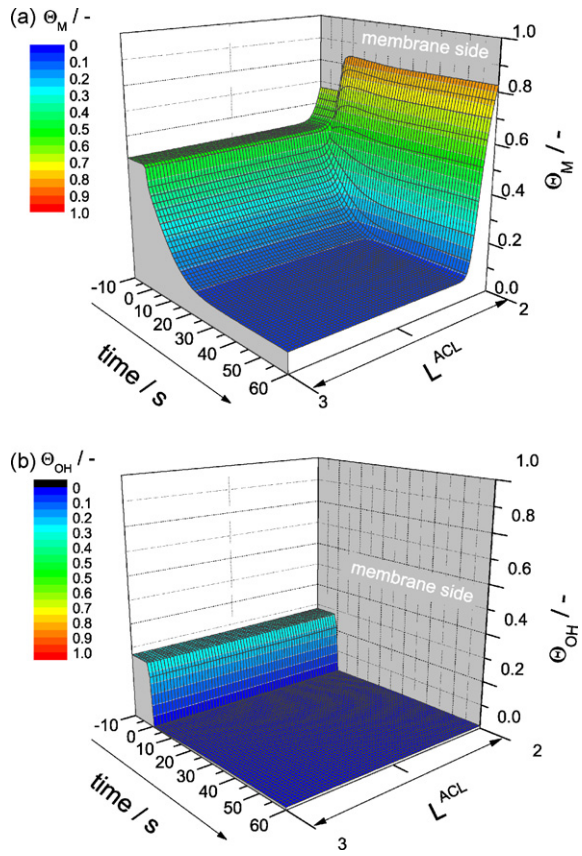

Fig. 13. Transients of the surface coverage of methanol and *OH*-species on the anode after current interruption show an insufficient bi-functional mechanism of the MOR, observable in a vanishing *OH*-coverage at OCV. (a) After current interruption the methanol coverage decreases from about 0.5 to 0.1 within 25 s due to *CO* poisoning. (b) A low and homogeneous coverage of *OH*-species of about 0.19 is observed before CI, decreasing rapidly at no-load condition.

the electrode potential is high enough to dissociate water. Thus the *OH* surface coverage is about 27% and the *CO* surface coverage is about 48%. After current interruption the anode electrode potential first remains stable for some milliseconds due to double layer discharging, than decrease to low values. With a small time delay the *OH* surface coverage decreases too. At this point the bi-functional mechanism comes to rest and thus the *CO* coverage increases, leading to a strong catalyst poisoning that makes the electrode potential very sensitive to a parasitic oxygen reduction reaction. Thus, after approx. 3 s the potential increases again.

3.3. Local analysis

The advantage of using such a detailed kinetic model is to provide the opportunity to determine the local conditions within the fuel cell such as surface coverage of adsorbed intermediates, concentrations and potentials. In the following a local analysis of the transients of certain solving variables after a current interruption from a current density of 0.1 A cm^{-2} for a Pt-cathode catalyst is made.

Fig. 13 shows the transients of the distributed methanol Θ_M and hydroxyl ion Θ_{OH} surface coverage in the anode catalyst layer. Under load ($t = -10\,\text{s} \ldots 0\,\text{s}$) the methanol coverage is nearly homogeneous within the ACL at a value of 0.5, with a small increase in the region of the membrane interface (Fig. 13(a)). This increase at the interface can be attributed to the oxygen crossover. A relative smooth transient to a lower value of 0.1 is observed after current interruption ($t > 0$), except at the membrane interface. Steady-

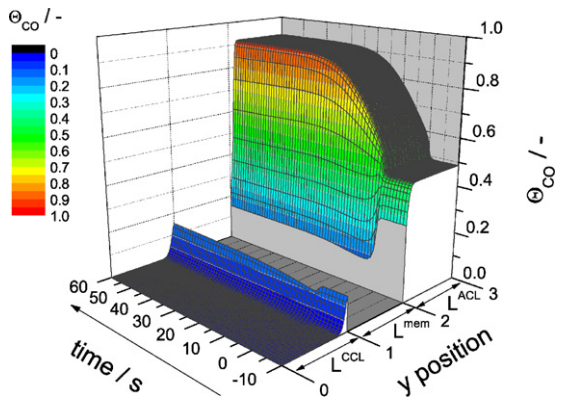

Fig. 14. Transients of the *CO*-coverage after CI. The *CO*-coverage on the anode raises from 0.5 to 0.9. The small *CO*-coverage on the cathode side at the interface to the membrane is hardly influenced by the CI.

state is reached after about 25 s. At no-load condition the coverage at the membrane interface increases from 0.68 to 0.83, leading to a steep gradient near the interface. This increase indicates an insufficient adsorption rate of methanol under load. The coverage of *OH* on the Ru-sites shows a very homogeneous distribution within the ACL (Fig. 13(b)), with a value of about 0.19 under load. The coverage decreases rapidly within 3 s to almost zero when turning to no-load because the water dissociation rate at low anode overpotential is insufficient to maintain a high coverage.

The phenomena of the steep gradient of methanol coverage near the membrane interface can be explained by the coverage of carbon monoxide. Fig. 14 shows the lapse of the carbon monoxide at the cathode and anode. A low coverage is observed on the cathode side near the membrane interface. The coverage on the cathode is almost stable in time after CI, indicating a relative constant parasitic MOR independent on the load conditions as long as no methanol mass transport limitation is present on the anode side. Since on the cathode the heterogeneous reaction with oxygen is the only process for a further oxidation of the adsorbed *CO* to CO_2, the assumed rate constant of this reaction has a strong influence on the degree of *CO*-poisoning of the CCL. Here, a sufficient rate constant is assumed to prevent a high catalyst blocking. This assumption could be too conservative, because the impact of catalyst poisoning might even be underestimated and could lead to a deteriorated electrode potential. Thus, measuring surface coverages by special in situ characterization techniques is essential to adjust the rate constant. On the anode side the same heterogeneous reaction is allowed for oxygen permeating through the membrane. Therefore, a steep decrease of Θ_{CO} is observed near the membrane interface which in turn leads to free Pt-sites for the adsorption of methanol, establishing the increasing Θ_M. The coverage of *CO* slowly increases after CI within the electrode, since as already mentioned not sufficient *OH*-ions are provided from the Ru-sites at low overpotentials. The anode catalyst gets poisoned.

The consumption of methanol due to the MOR is depicted in Fig. 15(a). A homogeneous MOR with a small increase near the membrane interface is shown in agreement with the distribution of Θ_M (see Fig. 13(a)), indicating a constant overpotential within the CL. After CI, the reaction stopped abruptly in the ACL, except for a small region near the membrane interface where the MOR has to counterbalance the still present parasitic ORR.

The parasitic MOR on the cathode side is depicted in Fig. 15(b). It shows that methanol is oxidized within the first 10% of the catalyst layer with a high rate, increasing after CI due to increasing methanol crossover, depicted in Fig. 16(a)). The distribution of the methanol concentration within the fuel cell shows clearly that a high methanol permeability of the membrane in combination with a low methanol diffusivity in the GDL results in a relative low methanol concentration in the ACL, even at no load condition. Hence, it can be concluded that a DMFC anode always suffers from mass transport limitations.

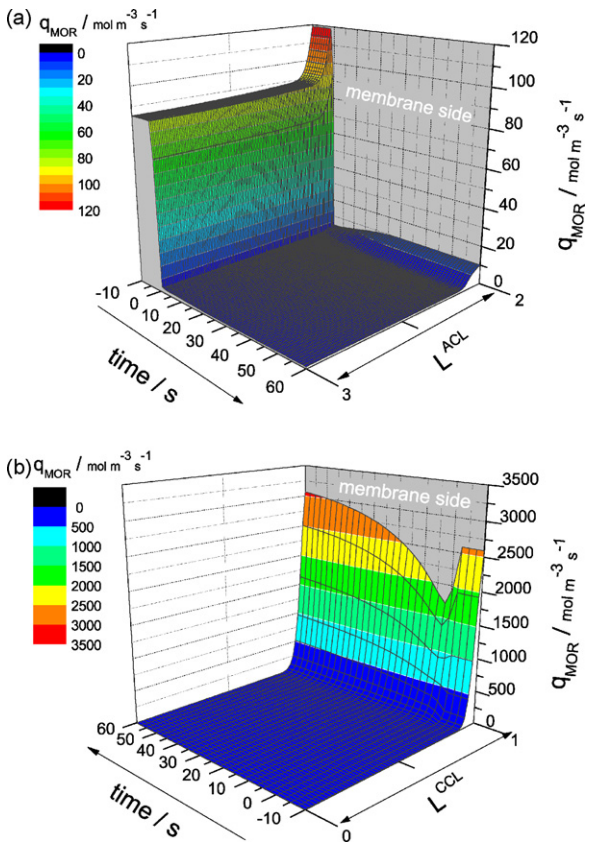

Fig. 15. The time evolution of the methanol consumption in the anode and cathode catalyst layer due to the MOR after current interruption at time $t = 0$ s is shown. (a) The simulation predicts a nearly homogeneous methanol consumption within the anode catalyst layer except near the membrane interface where an increase is observed due to oxygen crossover. (b) A very high parasitic current within the first 10% of the cathode CL is observed. After CI the parasitic current droped followed by an asymptotic increase.

The transient oxygen consumption by the ORR after CI within the CCL is depicted in Fig. 16(b). Under load a minimum of q_{ORR} is observed at the interface to the membrane due to the reduced number of active sites which are not blocked by *CO* (see Fig. 14). The minimum of q_{ORR} is also present near the membrane interface at no-load condition. Directly after current interruption, the ORR shows a sharp decline, followed by a smooth increase. This increase is caused by counterbalancing the increasing parasitic MOR due to increasing methanol crossover as already shown before in Fig. 16(a). A comparison of the oxygen consumption before (around 750 mol m^{-3} s^{-1}) and after CI (around 430 mol m^{-3} s^{-1}) at steady-state shows the high parasitic current at OCV.

By using a methanol tolerant cathode catalyst such as $RuSe_x$ the electrochemical conditions on the anode side are not affected, as shown in Fig. 10 for the anode overpotential. But taking a look on the cathode a completely different situation is predicted by the model with regard to the methanol distribution and the resultant methanol and oxygen surface coverages.

In Fig. 17 the methanol concentration distribution within the cell is depicted, showing a considerable amount of methanol in the cathode CL since the ORR selective catalyst oxidizes hardly methanol. Thus the methanol concentration in the CCL is determined by the boundary condition of methanol towards the gas diffusion layer. An arbitrary mass transport coefficient is used in the

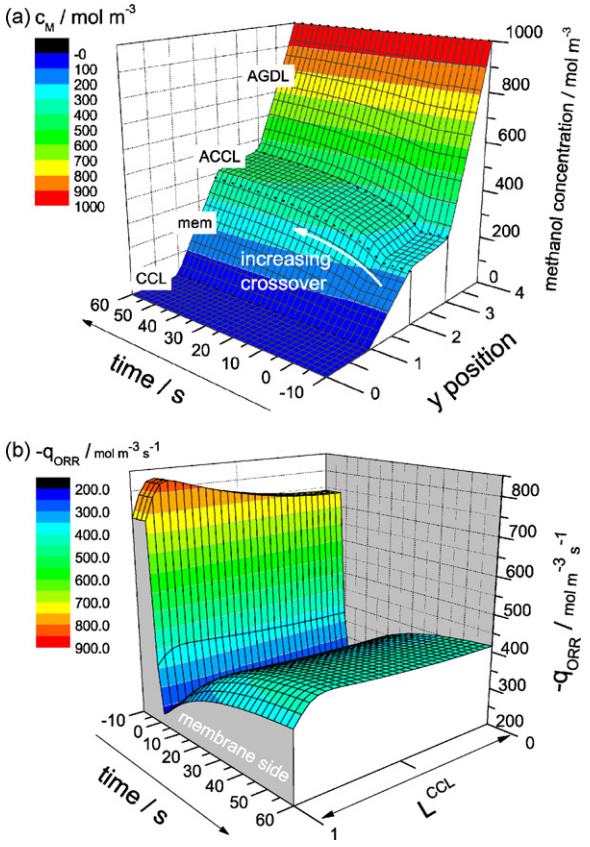

Fig. 16. Switching to no-load conditions leads to an increase of the methanol crossover and hence to an increase of the parasitic MOR that has to be counterbalanced in the CCL by the ORR. (a) Methanol concentration distribution within the cell after CI. Only a slight increase of methanol crossover is predicted, since the methanol distribution is governed by the parasitic MOR on the cathode throughout the experiment. (b) An increase of the ORR is observed after CI to counterbalance the parasitic MOR on the cathode side. The ORR is nearly homogeneous distributed in the CL with a small decline near the membrane interface due to *CO*-blocking.

formulation of a Cauchy boundary condition that could be identify for the model validation by measuring the methanol concentration in the cathode exhaust by mass spectroscopy or gas chromatography (not done in this work).

Since the adsorption process of methanol on the $RuSe_x$ catalyst is still allowed with only a marginal charge transfer reaction, a large fraction of the catalyst sites can be blocked by adsorbed

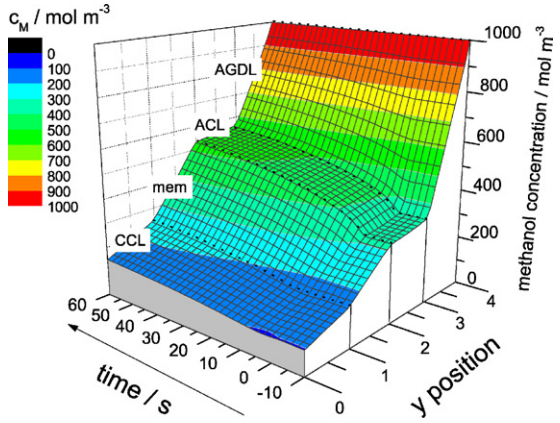

Fig. 17. Transient of the methanol concentration within the fuel cell after CI. The ORR selective $RuSe_x$ catalyst leads to a non-vanishing concentration in the CCL, whose value is determined by the outflow boundary condition.

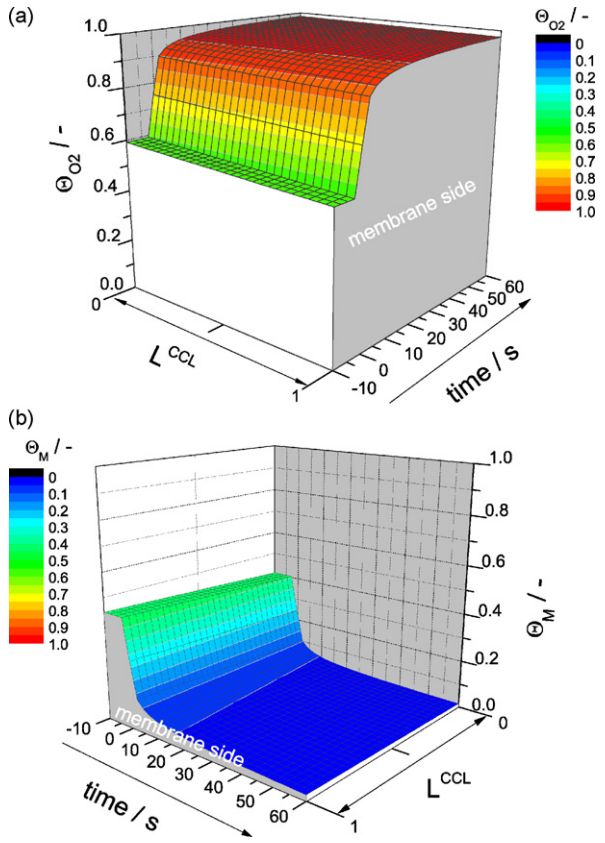

Fig. 18. The transient surface coverage of oxygen and methanol on the $RuSe_x$ catalyst shows a homogeneous distribution within the CCL. (a) The oxygen coverage increases after CI to almost 1.0. (b) The adsorbed methanol gets suppressed by oxygen after CI.

methanol molecules in case of fast adsorption rates and binding energies. For the oxygen this would imply a lowered amount of accessible active sites. Thus the choice of the involved constants for the ad-/desorption process is critical for modeling the cathode performance. Thus, it has to be emphasized again that in situ characterization techniques regarding the investigation of adsorbates are essential for parameter extraction by inverse modeling.

In the presented simulations the involved constants for the ad-/desorption processes are chosen under the assumption that the catalyst sites are mainly occupied by oxygen at no-load condition. As already mentioned, this strong assumption has to be proven by experimental measurements of surface coverages. The simulated transient of the oxygen coverage on the cathode after current interruption is plotted in Fig. 18(a). At 100 mA cm^{-2} the oxygen coverage has a value of 0.6, homogeneously distributed in the CL and after CI Θ_{O_2} increases to nearly 1. This shows that under load the consumption of oxygen by the ORR is too fast for the adsorption process to maintain the coverage in the range of 1. Under load methanol adsorbs on the free $RuSe_x$ sites, shown in Fig. 18(b).

4. Conclusion

The aim of the presented model was to find an interpretation of the so far unexplained anode undershoot, presented in the literature [1]. For this purpose a time-dependent complex fuel cell model based on a system of coupled PDEs describing the physical and electrochemical processes was developed. Essential for this model is the description of the anode kinetic by using a bifunctional mechanism, which can lead to *CO*-poisoning in case of a too slow *OH*-supply. This assumption alone is not sufficient for the

Table 1
Nomenclature and parameter values used for the simulation.

Symbol	Description	Value/Eq.	Unit	Ref.
Solving variables				
c_M	methanol concentration		mol m^{-3}	–
$c_{O_2}^{d,g}$	oxygen concentration (dissolved, gaseous)		mol m^{-3}	–
Θ_{CO}	surface coverage of carbon monoxide		–	–
Θ_M	surface coverage of methanol		–	–
Θ_{O_2}	surface coverage of oxygen		–	–
Θ_{OH}	surface coverage of hydroxyl ions		–	–
Φ^e	electronic potential		V	–
Φ^p	protonic potential		V	–
Physical constants				
F	Faraday constant	96,485	C mol^{-1}	–
R	gas constant	8.314	J K^{-1} mol^{-1}	–
Structural values				
L^{CL}	CL thickness	20×10^{-6}	m	measured
L^{GDL}	GDL thickness	430×10^{-6}	m	measured
L^{Mem}	membrane thickness	180×10^{-6}	m	measured
$\epsilon_{O_2}^{CL}$	volume fraction of open pores in CL	0.25	–	[39,30]
$\epsilon_{O_2}^{GDL}$	volume fraction of open pores in GDL	0.74	–	[40]
ϵ_i^{CL}	volume fraction of ionomer in CL	0.45	–	assumed
ϵ_i^{Mem}	volume fraction of ionomer in membrane	1	–	–
Physical properties, kinetic parameters and local variables				
$b_{ORR}(b_{ORR}^*)$	Tafel slope of the ORR	Eq. (9)	V	–
C_{DL}	double layer capacity	2×10^7	F m^{-3}	[32]
D_M^{CL}	methanol diffusion coefficient in CL	2.8×10^{-9}	m^2 s^{-1}	[24]
D_M^{GDL}	methanol diffusion coefficient in GDL	2.8×10^{-9}	m^2 s^{-1}	[24]
D_M^{Mem}	methanol diffusion coefficient in membrane @ 330 K	9.46×10^{-10}	m^2 s^{-1}	[41]
$D_{O_2}^d$	oxygen diffusion coefficient in ionomer	2.0×10^{-8}	m^2 s^{-1}	[42]
$D_{O_2}^g$	oxygen diffusion coefficient in gas phase	3.2×10^{-5}	m^2 s^{-1}	[43]
g_1	lateral interaction parameter	5	–	assumed
g_2	lateral interaction parameter	4	–	assumed
H	Henry constant	0.0254	–	[44]
k_{bleed}	rate constant for oxygen bleeding	3.03×10^{18}	mol m^{-3} s^{-1}	
$k_{CO,ox}$	rate constant for CO oxidation	1.25×10^5	mol m^{-3} s^{-1}	assumed
$k_{H_2O,red}$	rate constant for OH reduction	3.966×10^{11}	mol m^{-3} s^{-1}	assumed
$k_{H_2O,ox}$	rate constant for H_2O oxidation	7.6896×10^{19}	mol m^{-3} s^{-1}	assumed
$k_{M,ads}$	methanol adsorption constant	2.3606×10^5	s^{-1}	assumed
$k_{M,des}$	methanol desorption constant	3.3696×10^3	mol m^{-3} s^{-1}	assumed
k_{MOR}^{Pt}	rate constant for the $MOR_{forward}$	8.3×10^{13}	mol m^{-3} s^{-1}	assumed
k_{MOR}^{RuSe}	rate constant for the $MOR_{forward}$	3.3×10^2	mol m^{-3} s^{-1}	assumed
k'_{MOR}	rate constant for the $MOR_{backward}$	1×10^{-12}	mol m^{-3} s^{-1}	assumed
k_{ORR}^{Pt}	rate constant for the ORR	1.5×10^{-9}	mol m^{-3} s^{-1}	assumed
k_{ORR}^{RuSe}	rate constant for the ORR	1.5×10^{-13}	mol m^{-3} s^{-1}	assumed
$k_{O_2,ads}$	oxygen adsorption constant	7.4×10^6	s^{-1}	assumed
n_{act}	number of transfered electrons	1	–	[23]
n_{ORR}	number of transfered electrons	4	–	–
n_{MOR}	number of transfered electrons	4	–	[23]
n_{COOR}	number of transfered electrons	1	–	[23]
q_{ORR}	source/sink due to ORR	Eq. (8)	mol m^{-3} s^{-1}	-
$q_{O_2,ads}$	source/sink due to oxygen adsorption	Eq. (11)	mol m^{-3} s^{-1}	–
q_{MOR}	source/sink due to MOR	Eq. (12)	mol m^{-3} s^{-1}	–
$q_{M,ads}$	source/sink due to methanol adsorption	Eq. (14)	mol m^{-3} s^{-1}	–
q_{act}	source/sink due to water activation	Eq. (15)	mol m^{-3} s^{-1}	–
q_{COOR}	source/sink due to COOR	Eq. (18)	mol m^{-3} s^{-1}	–
q_{bleed}	source/sink due to oxygen bleeding	Eq. (20)	mol m^{-3} s^{-1}	–
s_{GDL}	saturation	0.55	–	estimated
s_{CL}	saturation	0.18	–	estimated
α_{drag}	electro-osmotic drag coefficient	Eq. (27)	–	–
α_{act}	symmetry factor of the water activation	0.1	–	assumed
α_{COOR}	symmetry factor of the COOR	0.5	–	assumed
α_{MOR}	symmetry factor of the MOR	0.818	–	assumed
α_{ORR}	symmetry factor of the ORR	0.478	–	assumed
$\gamma_{c,a}$	cathode/anode catalyst loading	1.26/1.9	–	measured
$\Delta\Phi_{OH}^0$	reversible potential of the water activation	0.4	V	assumed
$\Delta\Phi_{MOR}^0$	reversible potential of the MOR	0.043	V	[45]
$\Delta\Phi_{ORR}^0$	reversible potential of the ORR	1.23	V	[45]
$\Delta\Phi_{COOR}^0$	reversible potential of the COOR	0.346	V	assumed
Γ_{Pt}	active site density	78.15	mol m^{-3}	assumed
Γ_{Ru}	active site density	78.15	mol m^{-3}	assumed
λ	water content of ionomer	22	–	
σ_e	electrical conductivity	500	S m^{-1}	[46]
Ω_{O_2}	oxygen transfer coefficient	1×10^{-3}	m s^{-1}	assumed
Ω_M	methanol transfer coefficient	1×10^{-5}	m s^{-1}	assumed
Operating conditions				
T	operating temperature	354.15	K	measured

prediction of an anode potential undershoot since the anode has to be under load even if no external current is drawn. Accounting for a low oxygen crossover through the membrane seems to be obvious but is so far not described in the literature. The simulations show that a small amount of oxygen on the anode is actually enough for deteriorate the anode potential.

The description of the kinetics by means of exponential functions (Butler–Volmer approach) leads to a highly non-linear PDE system, that is numerically not easy to be solved. Since the simulations show that certain solving variables are nearly constant in y-position within the model domain and therefore do not have to be spatially resolved, the complexity of the model can be reduced.

Some kinetic parameters as used for the new approaches presented here are not described in the scientific literature. Therefore some parameters of the model had to be assumed.

At current status the model does not enforce the claims of an exact prediction of the operating state of a DMFC since there is a lack of information in experimental data for the model validation. Nevertheless the model identifies the determining loss mechanism of a DMFC:

- mixed potential formation on both electrodes and the resulting low OCV,
- poisoning effects of the catalyst layers and their dynamic effects on the electrode potentials.

The model predicts qualitative the characteristics of the polarization curves, the temperature dependent OCV and the potential relaxation curve after CI. Further experimental results are necessary for model validation, in particular information about surface coverages of the intermediates is required, since they have a strong influence on the electrode polarization. The measured interrelationship of the steady-state current and overpotential is not sufficient for the validation of such a complex model. For a better parameter extraction the next step should be the application of the model towards the simulation of electrochemical impedance spectroscopy in combination with in situ measurement techniques such as spectroscopy techniques like X-ray adsorption spectroscopy (XAS), Fourier-transformations-IR-spectroscopy (FTIR) or Differential Electrochemical Mass Spectroscopy (DEMS).

5. Nomenclature and parameter list

See Table 1.

References

[1] D. Gerteisen, J. Appl. Electrochem. 37 (12) (2007) 1447–1454.
[2] T. Iwasita, Chapter 41: Methanol and CO electrooxidation, in: W. Vielstich, H. Gaststeiger, A. Lamm (Eds.), Handbook of Fuel Cells, vol. 2, John Wiley and Sons, Chichester, 2003, pp. 603–624.
[3] V.A. Paganin, E. Sitta, T. Iwasita, W. Vielstich, J. Appl. Electrochem. 35 (2005) 1239–1243.
[4] H. Dohle, R. Jung, N. Kimiaie, J. Mergel, M. Müller, J. Power Sources 124 (2003) 371–384.
[5] X. Zhao, X. Fan, S. Wang, S. Yang, B. Yi, Q. Xin, G. Sun, Int. J. Hydrogen Energy 30 (2005) 1003–1010.
[6] V. Silva, J. Schirmer, R. Reissner, B. Ruffmann, H. Silva, A. Mendes, L. Madeira, S. Nunes, J. Power Sources 140 (2005) 41–49.
[7] C. Eickes, P. Piela, J. Davey, P. Zelenay, J. Electrochem. Soc. 153 (1) (2006) A171–A178.
[8] K. Lee, O. Savadogo, A. Ishihara, S. Mitsushima, N. Kamiya, K. Ota, J. Electrochem. Soc. 153 (1) (2006) A20–A24.
[9] U. Krewer, K. Sundmacher, J. Power Sources 154 (2005) 153–170.
[10] K. Scott, A. Shukla, C. Jackson, W. Meuleman, J. Power Sources 126 (2004) 67–75.
[11] F. Seland, R. Tunold, D.A. Harrington, Electrochim. Acta 51 (2006) 3827–3840.
[12] Z. Jusys, J. Kaiser, R. Behm, Electrochim. Acta 47 (22–23) (2002) 3693–3706.
[13] X. Xia, T. Iwasita, F. Ge, W. Vielstich, Electrochim. Acta 41 (5) (1996) 711–718.
[14] T. Vidakovic, M. Christov, K. Sundmacher, J. Electroanal. Chem. 580 (1) (2005) 105–121.
[15] L. Jörisson, V. Gogel, J. Kerres, J. Garche, J. Power Sources 105 (2002) 267–273.
[16] R. Jiang, J. Electrochem. Soc. 153 (8) (2006) A1554–A1561.
[17] J. Kallo, J. Kamara, W. Lehnert, R. von Helmolt, J. Power Sources 127 (2004) 181–186.
[18] H. Tributsch, M. Bron, M. Hilgendorff, H. Schulenburg, I. Dorbandt, V. Eyert, P. Bogdanoff, S. Fiechter, J. Appl. Electrochem. 31 (2001) 739–748.
[19] R. Koffi, C. Coutanceau, E. Garnier, J.-M. Léger, C. Lamy, Electrochim. Acta 50 (2005) 4117–4127.
[20] H. Yang, C. Coutanceau, J.-M. Lger, N. Alonso-Vante, C. Lamy, J. Appl. Electrochem. 576 (2005) 305–313.
[21] P. Argyropoulos, K. Scott, W. Taama, J. Power Sources 87 (2000) 153–161.
[22] P. Argyropoulos, K. Scott, W. Taama, Electrochim. Acta 45 (2000) 1983–1998.
[23] M. Shivhare, C. Jackson, K. Scott, E. Martin, J. Power Sources 173 (2007) 240–248.
[24] J. Ge, H. Liu, J. Power Sources 160 (2006) 413–421.
[25] W. Yang, T. Zhao, Electrochim. Acta 52 (2007) 6125–6140.
[26] X. Liu, H. Guo, F. Ye, C. Ma, Electrochim. Acta 52 (11) (2007) 3607–3614.
[27] E. Vilar, R. Dougal, J. Power Sources 169 (2007) 276–287.
[28] T. Frelink, W. Visscher, J.A.R. van Veen, Langmuir 12 (15) (1996) 3702–3708.
[29] K. Scott, P. Argyropoulos, J. Power Sources 137 (2) (2004) 228–238.
[30] F. Jaouen, G. Lindbergh, G. Sundholm, J. Electrochem. Soc. 149 (4) (2002) A437–A447.
[31] M. Eikerling, A. Kornyshev, J. Electroanal. Chem. 453 (1–2) (1998) 89–106.
[32] D. Gerteisen, A. Hakenjos, J. Schumacher, J. Power Sources 173 (2007) 346–356.
[33] D. Gerteisen, T. Heilmann, C. Ziegler, J. Power Sources 187 (2009) 165–181.
[34] U. Krewer, A. Kamat, K. Sundmacher, J. Electroanal. Chem. 609 (2007) 105–119.
[35] M. Watanabe, S. Motoo, J. Electroanal. Chem. 60 (3) (1975) 275–283.
[36] S. Gottesfeld, J. Pafford, J. Electrochem. Soc. 135 (10) (1988) 2651–2652.
[37] T. Springer, T. Zawodzinski, S. Gottesfeld, J. Electrochem. Soc. 138 (8) (1991) 2334–2341.
[38] S. Eccarius, Approaches to passive operation of a direct methanol fuel cell, PhD thesis, Universität Karlsruhe (TU), 2007.
[39] J. Ihonen, F. Jaouen, G. Lindbergh, G. Sundholm, J. Electrochem. Soc. 149 (4) (2002) A448–A454.
[40] M.V. Williams, H.R. Kunz, J.M. Fenton, J. Electrochem. Soc. 151 (10) (2004) A1617–A1627.
[41] B. Garcia, V. Sethuraman, J. Weidner, R. White, R. Dougal, J. Fuel Cell Sci. Technol. 1 (2004) 43–48.
[42] S. Um, C.Y. Wang, K.S. Chen, J. Electrochem. Soc. 147 (12) (2000) 4485–4493.
[43] S. Um, C.-Y. Wang, J. Power Sources 156 (2006) 211–223.
[44] R. Sander, Compilation of Henry's law constants for inorganic and organic species of potential importance in environmental chemistry, http://www.mpch-mainz.mpg.de/sander/res/henry.html.
[45] P. Kurzweil, Brennstoffzellentechnik: Grundlagen, Komponenten, Systeme, Anwendungen, Vieweg+Teubner Verlag, 2003.
[46] W. Sun, B.A. Peppley, K. Karan, Electrochim. Acta 50 (16–17) (2005) 3359–3374.